Development of the GEANT4 Simulation for the Compton Gamma-Ray Camera

Ryuichi Ueno

Prepared by:

Calian Technologies Ltd.
340 Legget Dr. Suite 101, Ottawa, ON K2K 1Y6

Project Manager: Pierre-Luc Drouin
Contract Number: PA15003 (W0046-16-088)
Contract Scientific Authority: Pierre-Luc Drouin

DRDC-RDDC-2016-C138

March 2016

Table of contents

List of tables

List of figures

1 Introduction to Compton Imager

A Compton gamma imager is useful for detecting and localizing the source of gamma-emitting radioactive sources. A project to develop the imager for security, emergency response and military use was funded by Department of National Defence (DND), and with collaboration with National Research Council (NRC) and Natural Resources Canada (NRCan).

A Compton imager mainly consists of two layers of gamma-ray detectors, each layer segmented in x-y plane for position localization. If it is assumed that the gamma ray from the source scattered once in the front plane (scatter layer), and fully absorbed in the back plane (absorber layer), then the angle θ_C between the incident direction and the direction of the scattered gamma ray can be calculated up to a cone: [1]

$$\cos(\theta_C) = 1 + m_e c^2 \left[\frac{1}{E_{total}} - \frac{1}{E_{absorber}} \right] \tag{1}$$

Overlap of several of these "Compton cones" gives the location of the source (See Figure 1 for illustration).

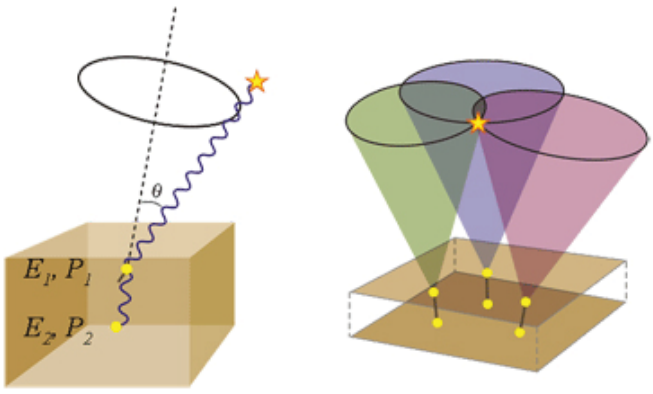

Figure 1: *Schematic illustration of a Compton camera. Two layers of gamma-ray detectors and several overlaps of Compton cones can provide the location of initial gamma-ray source.*

NRC has assembled a laboratory set up consisting of two scatter layers, each consisting of 9 by 9 array of thallium-doped cesium iodide (CsI(Tl)) crystals, and an absorber layer of 10 by 10 array of thallium-doped sodium iodide (NaI(Tl)) crystals. It was successful in localizing several known sources (^{137}Cs, ^{113}Sn and ^{22}Na of 1 mCi activity at a distance of 10 m away from the detector), as well as to measure and characterize detector responses. [2, 3] A GEANT4 simulation was written to simulate

this experimental setup, with intention to assess the detector response at different geometry configurations and various scenarios. [4]

This contract report continues the work to: further develop the simulation (Section 2); perform cross checks with independently-developed simulation by the NRC group (Section 3); develop image reconstruction algorithms (Section 4); and advance the framework to possible military scenarios (Section 5). Section 6 concludes the report.

2 DRDC Imager Simulation

Initial effort of the DRDC simulation was documented in [4]. GEANT4 framework [5, 6] was chosen for the Monte Carlo (MC) simulation. The detector geometry was designed to replicate the NRC laboratory setup (See Figure 2a), with the "source" (simulated by a particle gun emitting mono-energetic gamma rays in a cone in the direction of the detector) placed at a distance away in a volume filled with air (See Figure 2b). Particle interactions are modelled by GEANT4, and event information book keeping is also handled by the simulation framework.

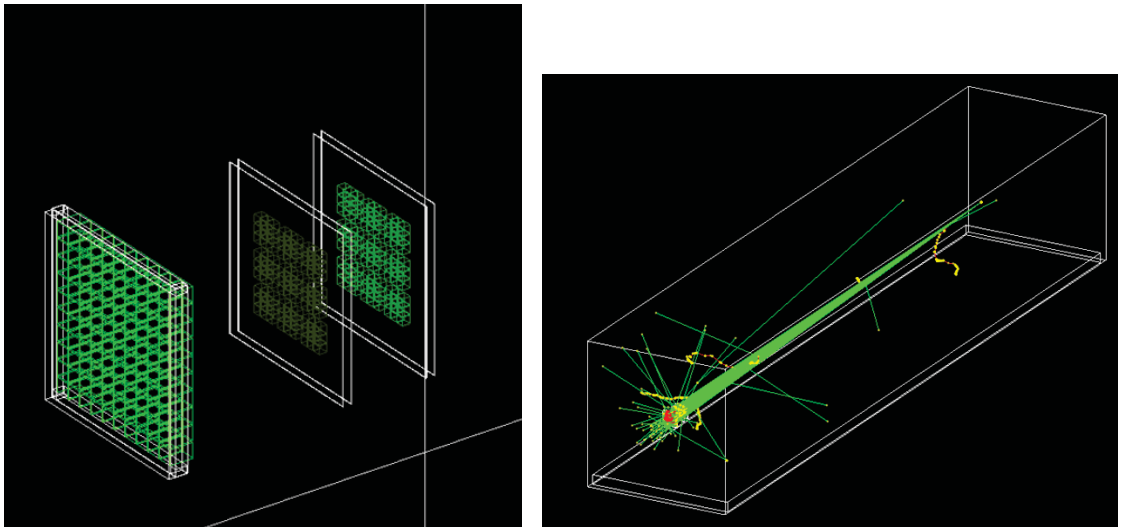

(a) ***(b)***

Figure 2: *Visualization of the original DRDC imager simulation. (a) depicts the close-up view, where the detector cell structure is visible (b) depicts the gamma rays traversing through the world volume and interacting with the detector cells.*

2.1 Improvement to the DRDC Simulation

Several improvements to the original DRDC simulation were made before proceeding with further analysis. GEANT4 version 4.9.6 and 4.10.1 are used for the remainder of the report. [1] The improvements are described below.

[1] Version 4.10.1 showed discrepancies in the ARM distribution. The disagreement was only visible with large-statistics sample, and only uncovered in February 2016. The source of this discrepancy is still unresolved and under investigation.

2.1.1 Improvement to the Output File

Original simulation produced an output in ASCII file format. This has limited flexibility and robustness in post-simulation analysis, and provides no file compression that could be advantageous for longer simulations.

Instead, the simulation is updated to produce an output in a ROOT analysis format [7] with branches that hold event-by-event information such as energy, position, and detector cell indices, as well as the ability to build and store histograms. The ROOT output file can then be read using a C++ library by post-simulation analyses.

2.1.2 Improvement to the Particle Generator

The particles are generated by a so-called "particle gun" within the GEANT4 framework, which can simulate the decay of an isotope by a production of distribution of γ rays in a cone directed toward the detector. The limitation of this method is that there can only be one particle gun per simulation run. This limitation results in inability to simulate scenarios with multiple point sources or extended sources (for example, radioactive spills or plumes).

Instead, General Particle Source (GPS, a part of GEANT4 framework) [8] is employed. This enables definition of an arbitrary volume of sources. Using an input macro (rather than hard-coded configurations), a user can define the number and

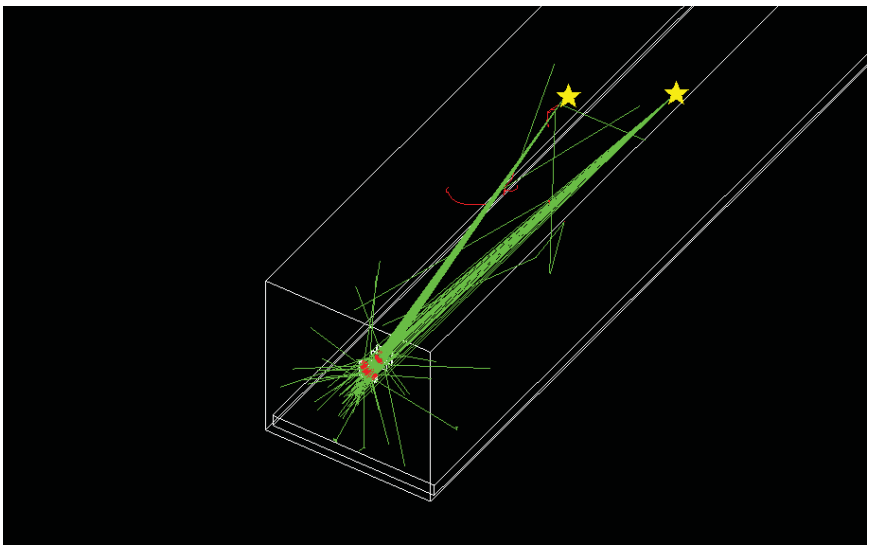

Figure 3: *Visualization of simulation of multiple sources using General Particle Source (GPS). The scene includes two source locations, indicated by yellow stars, producing gamma rays directed towards the detector.*

volume of the sources per run. An example visualization of two sources is shown in Figure 3.

2.1.3 ROOT Analysis code

The post-simulation analysis code was not a part of the original simulation package in [4]. It is written in ROOT framework, a commonly-used data analysis environment that is also used by the NRC group. This commonality is important in the scope of comparison studies (see Section 3) and cross checks. The code obtains event information from the output ROOT file produced by the GEANT4 simulation as described in Section 2.1.1.

The analysis performs event selection as described in [2], and subsequently produces energy spectra, angular resolution, and back projection images. The results are shown in the subsequent section.

3 Comparison with the NRC Simulation

NRC has independently developed a GEANT4 simulation of the Compton imager, which has been internally validated against a separate MC simulation based on EGSNRC [9] and the experimental data. Naturally, comparison of DRDC GEANT4 simulation and NRC simulation is sought, and results are presented in the following subsections.

3.1 Identified Differences between DRDC and NRC Simulations

Through various thorough cross checks, two key differences were identified. Updates to the DRDC simulation were made to consolidate these differences before proceeding with the comparison study. They are summarized below:

3.1.1 Detector Definitions

The NRC detector definitions more closely resemble the actual detector (See Figure 4 for the updated geometry):

- The aluminum substructures surround each of the absorber cells instead of just

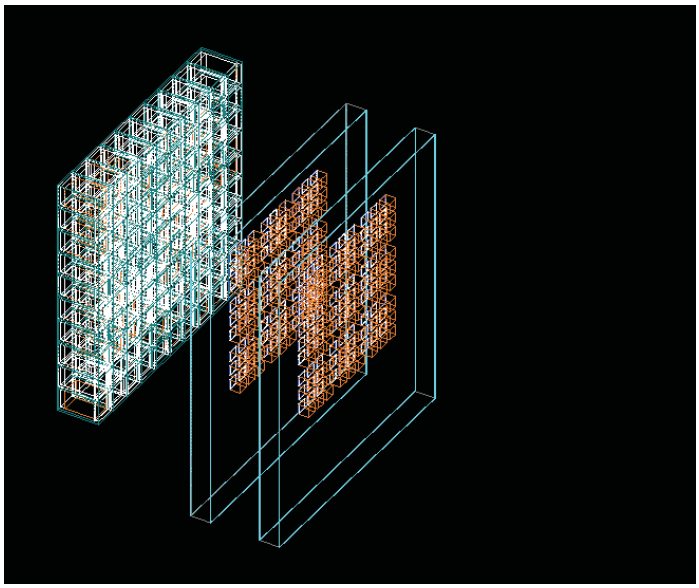

Figure 4: *An updated detector geometry with more realistic and detailed components. See text for the details of the updates to the detector geometry.*

the perimeter of the absorber layer as was approximated in the original DRDC simulation

- The Silicon Photomultipliers (SiPM) and the Photomultiplier Tubes (PMT) were not simulated in the original version. In the updated definition, they are approximated by a thin layer of glass with a gold film
- Plastazote foam fills the gap between the scatter detector cells (the gap was filled with air in the original simulation), between the two carbon fibre plates.

3.1.2 The Physics Model

The physics model definitions used in the original DRDC simulation did not include low-energy interactions, thus did not simulate events whose energies were fully absorbed in the scatter layers. Although these low-energy events are rejected by subsequent event-selection processes, they are included for completeness of the simulation.

3.2 Comparison of Energy Spectra

For this comparison, 10 million gamma rays were directed toward the detector (approximately equivalent to 1000 second exposure of a 1 mCi source at 10 m away). For the comparison of energy spectra, only coincidence events are selected. Coincidence events are defined as events with non-zero energy deposit in exactly one cell in either one of the scatter layers, and exactly one in the absorber layer. This ensures the events have gone through a Compton scatter but also minimizes the chance of multiple-scattering events.

The updated DRDC simulation was compared with the NRC simulation code provided by the NRC group, which was compiled using the same machine and the same version of GEANT4 (4.10.1). Identical macro file that defines the input parameter to the simulation was also used for the two simulations.

Figure 5 shows the result of the comparison. In each plot, the ratio (middle) and the pull distribution (bottom - defined as $(n_1 - n_2)/\sigma$, where $\sigma = \sqrt{n_1 + n_2}$) are shown. As it can be seen, the two distributions agree well within the statistical fluctuations. To further quantify the agreement of the energy spectra, the projection of the pull distribution was fitted to a Gaussian, where the fitted parameter consistent with $N(0, 1)$ indicates good agreement. As it can be seen in Figure 6, a very good agreement is achieved.

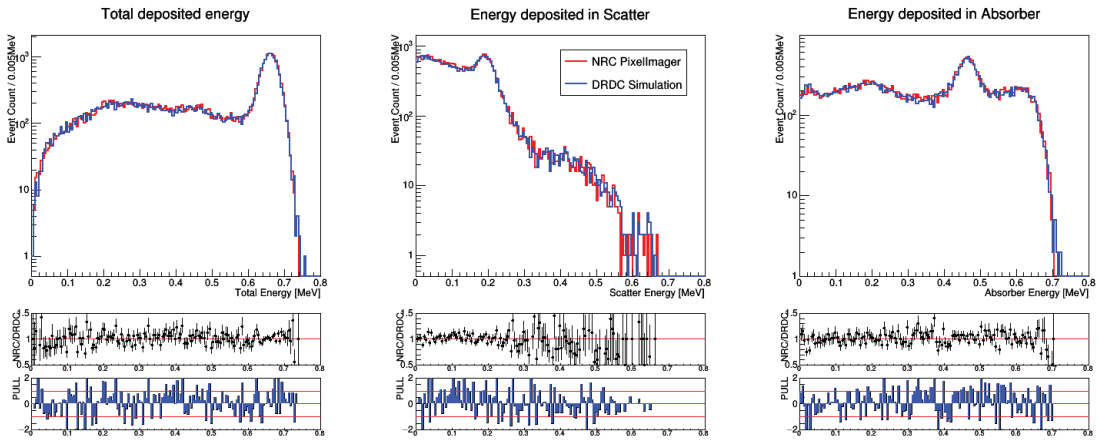

Figure 5: *Comparison of energy spectra of coincidence events from NRC simulation (red) and DRDC simulation (blue) after matching the differences identified in Section 3.1. Left plot shows the total energy spectrum; Centre plot shows the energy spectrum in the scatter layer, and; Right plot shows the energy spectrum in the absorber layer. All of the plots also show the ratio plots (middle row) as well as the pull (bottom row).*

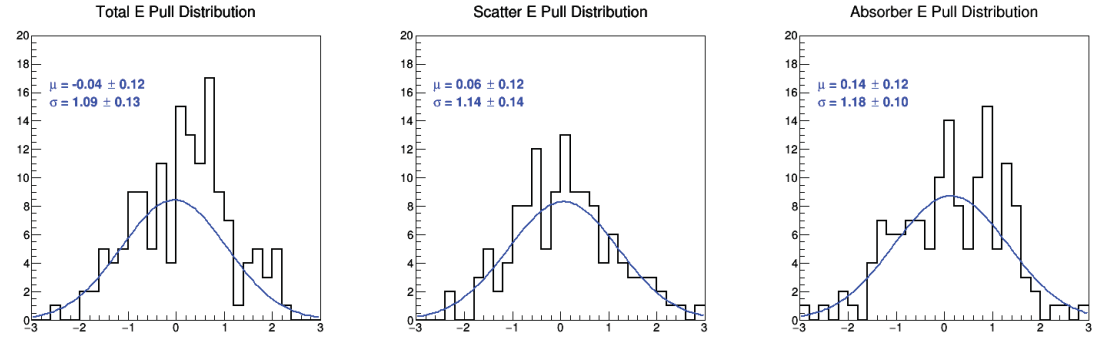

Figure 6: *Distributions of the pull from Figure 5. The distribution should follow a normal distribution $N(0,1)$ for two unbiased samples from the same parent distribution. Left, centre, and right show the pull distribution for total energy, scatter energy, and absorber energy, respectively.*

3.3 Comparison of Angular Resolutions

The angular resolution measure (ARM) is defined as the difference in reconstructed Compton angle θ_C^{reco} and the Compton angle assuming the true position of the source θ_C^{true}. [2] The ARM essentially is the measurement of the performance of the camera. For the comparison, in addition to selecting the coincidence events, the following selection criteria are applied:

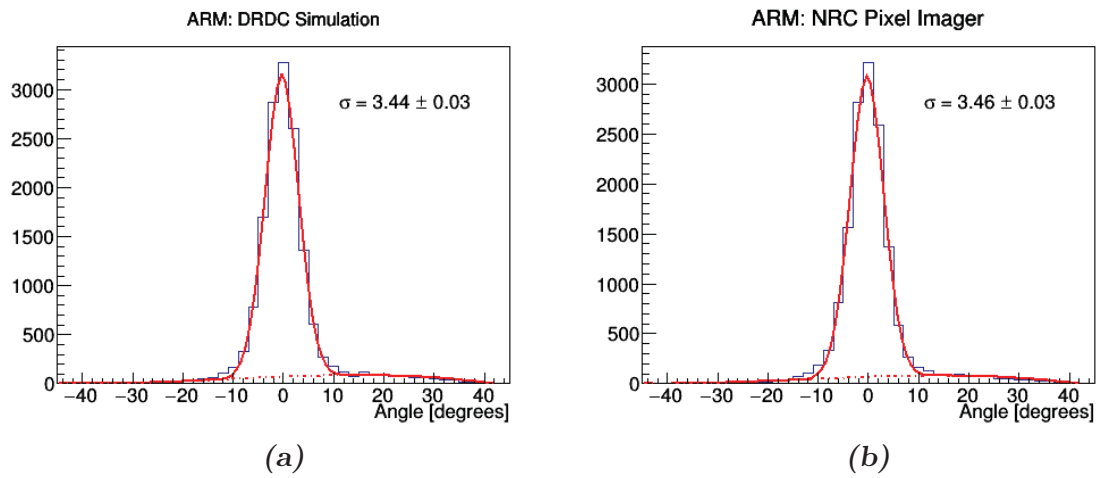

(a) *(b)*

Figure 7: *Distributions of Angular Resolution Measure (ARM) after the event selection. (a) ARM from the DRDC simulation after matching the differences identified in Section 3.1. (b) ARM from the NRC simulation. Each distribution is fitted with a Gaussian and a third-order polynomial.*

1. Reject backscatter events. Backscatter events refer to those that first interact with absorber material or the material surrounding the scatter layer *before* interacting with the scatter detector. The backscatter events have energy peaks that can be calculated from the Compton kinematics: [10]

$$E_{scat}^{bs} = \frac{E_{total}}{1 + 2E_{total}/m_e c^2}. \tag{2}$$

   For the ^{137}Cs source, this corresponds to $E_{scat}^{bs} = 184$ keV. To be conservative, events with $E_{scat} > 120$ keV are rejected.

2. Consider only events with total energy close to the photopeak energy. For ^{137}Cs, events with E_{total} outside the window 662 ± 40 keV are rejected (the window corresponds to about 6 %, equivalent to the measured FWHM of the energy resolution of the detector).

Figure 7 shows the comparison of ARM distribution. The distributions are fitted with a Gaussian with a third-order polynomial to eliminate the tail effect. The width of the Gaussian gives the resolution measure. As it can be seen from the figures, the fitted resolution measures agree within the uncertainty, and also consistent with [3].

Figure 8 shows the comparison of ARM and the reconstructed Compton angle for the two versions of GEANT4, using high-statistics sample (75 million gamma events). The disagreement in the ARM distribution can be seen in the ratio plot, where statistically significant deviation is visible between ±10 degree window. No disagreement is visible for Compton angle, or energy spectra (not shown).

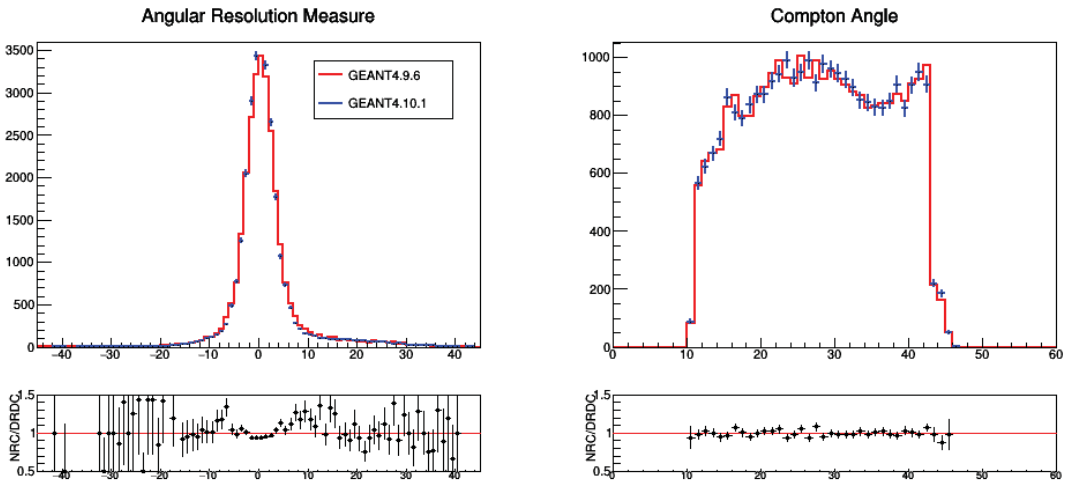

Figure 8: *Comparison of angular distributions: ARM (left) and reconstructed Compton angle (right), for the two GEANT4 versions: 4.9.6 (red) and 4.10.1 (blue). Statistically significant disagreement is observed for the ARM distribution. No disagreement is visible for Compton angle distribution.*

3.4 Conclusion from the Comparison Study

The comparison study of the two independently-developed GEANT4 simulations were conducted. As was just illustrated, the energy spectra and ARM are in good agreement between the two simulation codes. There exist disagreement in the ARM distribution for the two versions of GEANT4. However, the source of the disagreement is not yet known. Version 4.9.6 is validated with the EGSNRC simulation, thus is recommended over the newer version.

Instead of developing and maintaining two versions of the simulation software, it is decided to combine the two simulations and have one version. The code is expected to be version-controlled and hosted by NRC server (in progress). For the remainder of the report (and in the future), the merged simulation framework is used.

4 Image Reconstruction Algorithms

Localization of the sources is one of the main goals of the Compton imager. DRDC has taken a lead on exploring and reviewing possible image reconstruction algorithms. There exist several different algorithms developed and applied to Compton gamma ray detectors. Review and comparison of some of these methods, namely simple back-projection, two-cone backprojection, and list-mode minimum-likelihood expectation maximization are reviewed, and detailed in the subsequent sections. In addition, stochastic origin ensembles (SOE) is also being reviewed as another viable algorithm to be implemented for Compton imager. However, it is outside the scope of this report.

4.1 Simple Backprojection

Each Compton event is defined by a vector connecting the hit locations in the scatter and the absorber layers, and the Compton angle θ_C defined by Equation 1. These information can be plotted onto a 2D histogram defining angles in x- and y- directions. For each event, the location of the original source must lay on the circle. When several events are overlaid, the build-up of the common pixel give the more likely position of the source.

The Compton cones are in reality ellipses; they are circles only in angular space. This choice makes the calculation simpler. In addition, each cone is assumed to have its

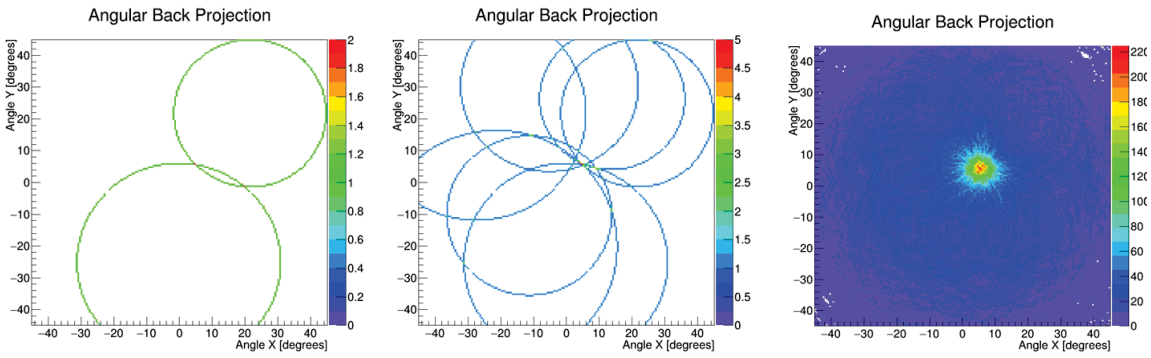

(a) *(b)* *(c)*

Figure 9: *An illustration of simple backprojection procedure. (a) Each Compton event produces a circle in 2-D angular space, where the centre of the circle is the direction of the vector connecting the hits in the scatter and the absorber layers, and the radius is defined by the Compton angle (Equation 1). (b) overlaying several rings will give a clearer idea of the location of the source. (c) summing over all events will produce an image with a peak indicating the location of the original source.*

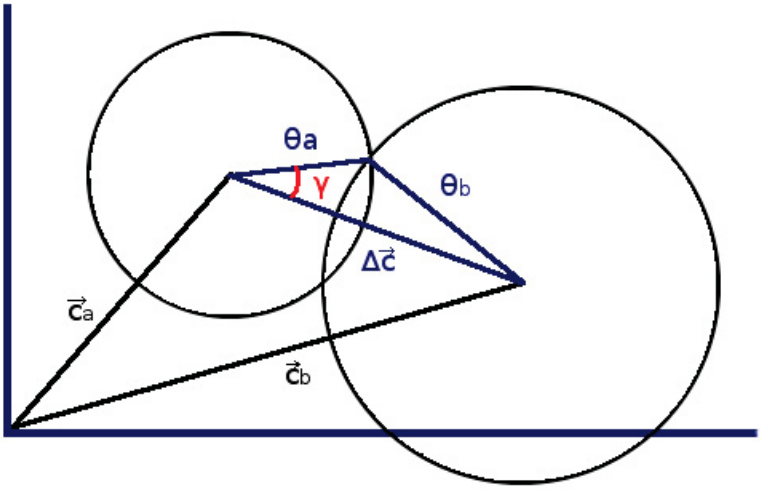

Figure 10: *An illustration of two-cone backprojection method. The method tries to find the intersections of two circles from two Compton events. See text for detailed explanation.*

apex set at the centre of the detector such that the centre of the backprojected circle is defined by the vector connecting the two detector hits. This assumption is valid when the detector dimension is negligible relative to the source distance.

This principle is illustrated in Figure 9. For this example, the source was placed 1 m off-axis at 10 m away (approximately 6 degrees off-axis). As it is depicted, this simple algorithm can provide a good idea of the location when many events are overlapped.

4.2 Two-Cone Backprojection

Instead of overlaying full cones as done by the simple backprojection, the two cone algorithm populates the histogram with only the intersections. To find the intersection between two cones projected onto θ_x - θ_y plane, the following steps are employed (See Figure 10):

1. Find the centre of the two cones, $\vec{c_a}$ and $\vec{c_b}$. Let θ_a and θ_b be the Compton angles for the two events
2. Find the difference of the two centres $\vec{\Delta}c$
3. Find the angle γ between $\vec{\Delta}c$ and the vector from center of the first cone to the

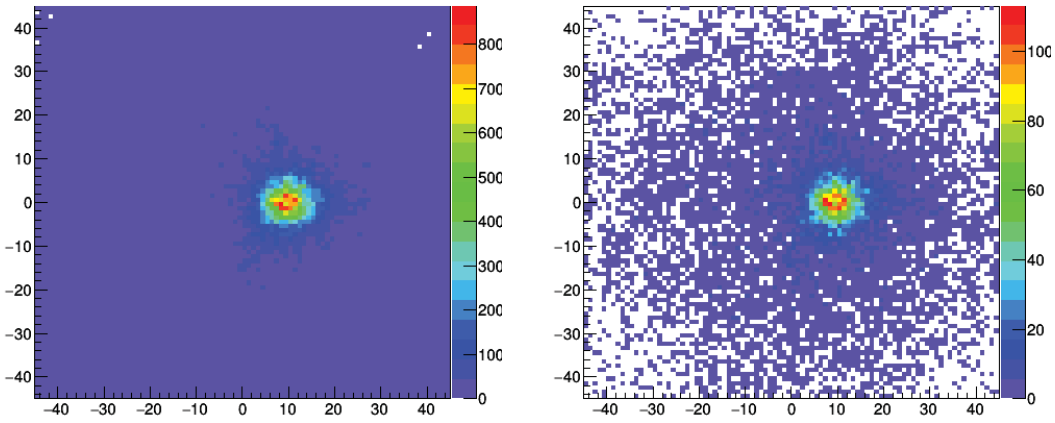

(a) ***(b)***

Figure 11: *Examples of two-cone backprojection method. (a) Two-cone backprojection with full-size loop. (b) Two-cone backprojection with moving window of size 10.*

intersection using the cosine law:

$$\gamma = \cos^{-1}\left[\frac{\theta_a^2 + |\vec{\Delta c}|^2 - \theta_b^2}{2\theta_a|\vec{\Delta c}|}\right]$$

4. Let $\vec{\theta}_{a\pm} = \vec{\Delta c}.Rotate(\pm\gamma)$ with $|\vec{\theta}_{a\pm}| = \theta_a$, then the two intersection points are given by:

$$\vec{c_a} + \vec{\theta}_{a\pm}$$

The algorithm calculates the intersection for each unique pair of cones in an event. Which results in loop of $\binom{N}{2}$ iterations for N measured events, which gets computationally expensive very quickly. If instead, a moving window of size w is used to find the intersections, then the number of iterations become $\binom{w}{2} \times (N - w)$.

The result for the case of a source placed 10 degree off-axis 10 m away are shown in Figure 11. As it can be seen, The core peak is largely unaffected by the moving window method, but reduces the noise on the outer edges of the image. See Section 4.4 for further evaluation of the moving window.

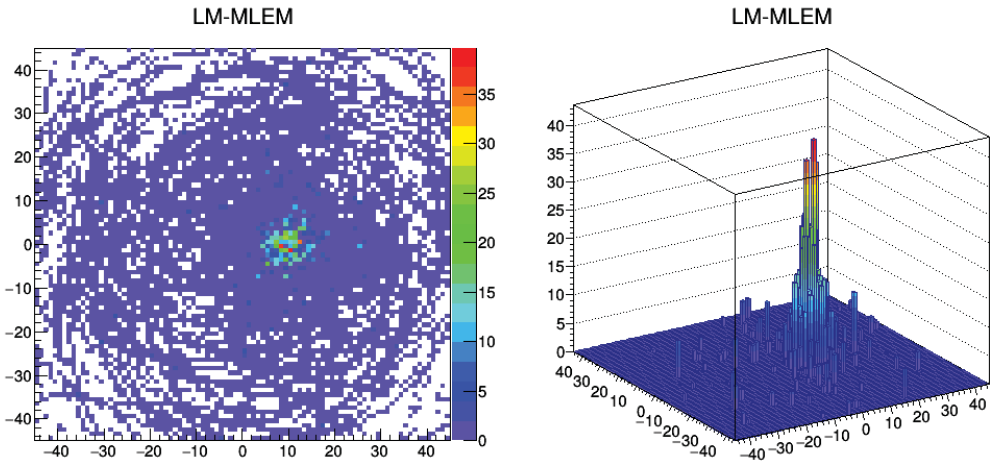

(a) *(b)*

Figure 12: *Reconstructed images from LM-MLEM. (a) 2-D representation (b) 3-D representation showing the peak corresponding to the location of the source.*

4.3 List-Mode Minimum-Likelihood Expectation Maximization (LM-MLEM)

If N measured projection data are obtained from a Compton imager, $A_1, \ldots, A_N$, where A_i consists of energy and position measurements in the detector for i-th event, and the intensity of pixelated image in pixel j is λ_j, then a likelihood function can be constructed as:

$$L(A_1, \ldots, A_N|\lambda) = \sum_{i=1}^{N} \ln \left[\sum_{j=1}^{M} p(A_i|\lambda_j) p(\lambda_j|\lambda) \right] \tag{3}$$

where $p(A_i|\lambda_j)$ is the probability that a γ emitted from pixel j is reconstructed in event A_i, and $p(\lambda_j|\lambda) = \lambda_j / \sum_n \lambda_n$ is the relative intensity of pixel j. Then, the intensity for each pixel λ_j can be iteratively computed using a commonly-used image reconstruction algorithm called list-mode MLEM: [11, 12, 13]

$$\lambda_j^{n+1} = \frac{\lambda_j^n}{s_j} \sum_{i=1}^{N} \frac{t_{ij}}{\sum_{k=1}^{M} t_{ik} \lambda_k^n} \tag{4}$$

where t_{ij} is the probability that a γ emitted from pixel j is reconstructed in event i $(= p(A_i|\lambda_j))$, and s_j is the sensitivity of the detector for pixel j.

The t_{ij} terms are calculated as a ratio of arc length of the Compton ring inside the pixel to circumference of the Compton ring for event i, and s_j term is set to unity

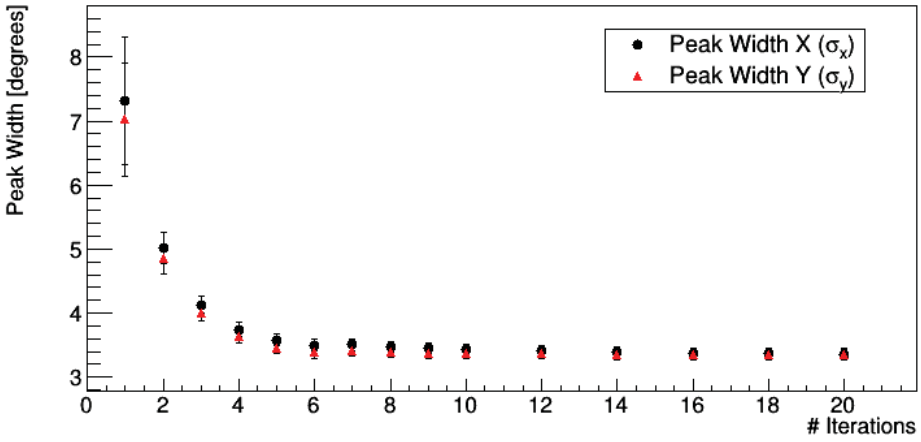

Figure 13: *A plot of width of the fitted Gaussian peak on an image from LM-MLEM as a function of number of iterations to be computed.*

for simplicity (i.e. ignore detector response). The results for a GEANT4 simulation of 1 million generated γ, with number of iterations $n = 100$ are presented in Figure 12. As it can be seen the algorithm is successful in reconstructing the peak.

There is no explicit criterion for number of iterations to be computed. However, as it can be seen in Figure 13 for the example case of a point source, whilst the improvement in the image quality (the width of the fitted Gaussian peak) is significant for the first few iterations, it becomes diminutive as a function of number of iterations to be processed. Therefore, in general, the iteration is stopped when the improvement in the likelihood function becomes small:

$$\frac{L(A|\lambda)^n - L(A|\lambda)^{n-1}}{L(A|\lambda)^n} < 0.1\% \tag{5}$$

where $L(A|\lambda)^n$ is computed from Equation 3 after n-th iteration. Typically, the image is converged after 10 to 20 iterations, depending on the complexity of the scenario.

4.4 Evaluation of Performance

4.4.1 Source Localization

In order to quantitatively identify the location of the peak for each of the methods described above, a bivariate Gaussian fit is employed, given by the function (ignoring x-y correlation):

$$f(x,y) = \frac{1}{2\pi\sigma_x\sigma_y} exp\left(-\frac{1}{2}\left[\frac{(x-\mu_x)^2}{\sigma_x^2} + \frac{(y-\mu_y)^2}{\sigma_y^2}\right]\right) \tag{6}$$

Method	μ_x	μ_y	σ_x	σ_y
Simple BP	9.840 ± 0.066	-0.084 ± 0.062	7.204 ± 0.096	6.991 ± 0.090
Two-cone BP	9.959 ± 0.049	-0.110 ± 0.047	4.180 ± 0.046	4.097 ± 0.049
LM-MLEM	10.004 ± 0.087	-0.117 ± 0.094	3.204 ± 0.069	3.218 ± 0.069

Table 1: *Result of the bivariate Gaussian fit to the reconstructed peak angle from the three reconstruction algorithms. There are four fit parameters as described by Equation 6*

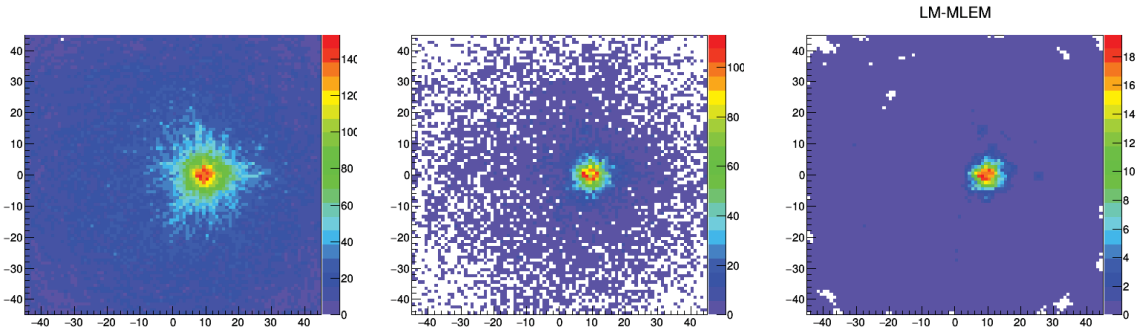

(a) ***(b)*** ***(c)***

Figure 14: *Comparison of output images for the reconstruction methods explored: (a) Simple backprojection method; (b) Two-cone backprojection method (moving window with $w = 10$); (c) LM-MLEM method (with smoothing applied).*

The fit to the means (μ_x and μ_y) and the widths (σ_x and σ_y) provide the quantitative measure of the location of the source. The results of the fit is provided in Table 1. From these angles, one can also reconstruct the (x,y) position as (given distance z away from the detector):

$$\begin{cases} x = z\tan(\theta_x) \\ y = z\tan(\theta_y) \end{cases}$$

Figure 14 shows the comparison of the three image reconstruction algorithms for 1 million generated γ at 10-degree off-axis. As evident from the figure and from Table 1, all three algorithms were successful in determining the source position.

It can also be seen that LM-MLEM can localize the position within half of the peak width of the simple back projection, while two-cone back projection improves the peak width by ∼40% compared to the simple back projection.

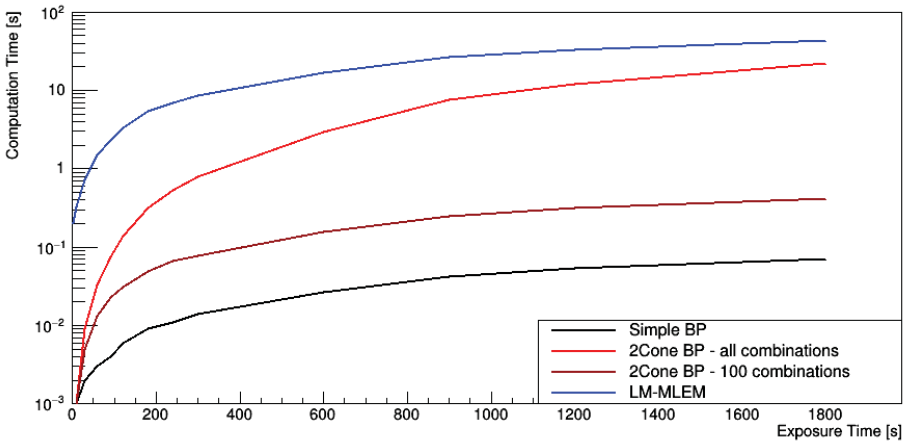

Figure 15: *Comparison of the computation time for the three image reconstruction algorithms as a function of exposure time.*

4.4.2 Computation Time

An ideal Compton imager is able to image and localize a source in real time. The goal is to accurately reconstruct the source as quickly as possible, therefore evaluation of computation time is an important criteria for these algorithms.

Figure 15 shows the comparison of the computation time for the tree image reconstruction algorithms. It can be seen that the simple backprojection is the quickest, and able to provide an image within fraction of a second, and LM-MLEM method takes more than a second even with a short exposure time. Two-cone backprojection with or without moving window, as described in Section 4.2, has big impact on computation time at longer exposure time. The moving window can image within fraction of a second, while two-cone backprojection without the moving window approaches time taken for LM-MLEM algorithm.

4.4.3 Robustness of the Algorithms

Simple back projection, while simplistic and computationally cheap, has relatively poor resolution (as demonstrated in Section 4.4.1). Two-cone back projection improves on the resolution and also computationally efficient, however the algorithm by construction assumes a static point source, therefore not expected to perform well in scenarios involving an extended source or a moving source. LM-MLEM algorithm makes no such assumptions, therefore expected to outperform the other two algorithms in image-quality at the expense of longer computational time (as demonstrated in Section 4.4.2).

Therefore, simple back projection is useful in "discovery mode", where the main objective is to identify the existence of a source, and LM-MLEM is more useful in "imaging mode" where a higher-resolution image is needed with longer exposure time. Two-cone algorithm is a useful alternative in both cases where the source is known to be static and/or well-localized.

5 Additional Updates to the DRDC Simulation Package

5.1 Mission-Ready, Portable Design Prototype

So far the laboratory detector design, consisting of two scatter layers and an absorber layer, was modelled and evaluated. However, this design is not practical for field use. Therefore a mission-ready design, aimed for portability and ease-of-use is also under development. This mission-ready prototype will have smaller dimension, and only employs one scatter layer, as well as use of SiPM for all detector cells. The difference is detailed in Table 2.

Design	Laboratory	Mission-Ready
Scatter Layer	9x9x2 grid of CsI(Tl) (1.35x1.35x1.35) cm^3	4x4x1 grid of CsI(Tl) (1.35x1.35x1.35) cm^3
Absorber Layer	10x10x1 grid of NaI(Tl) (2.5x2.5x4.0) cm^3	4x4x1 grid of CsI(Tl) (2.8x2.8x2.8) cm^3
Photodetector	SiPM (Scatter) PMT (Absorber)	SiPM (Scatter) SiPM (Absorber)

Table 2: *Difference between the laboratory detector design and the mission-ready detector design.*

In order to evaluate the performance of the new design, an updated geometry is implemented into the GEANT4 simulation. A visualization of the new geometry is depicted in Figure 16a.

This design is also modular in nature, so it could be stacked to have a larger active area, providing better sensitivity. This is useful, for example, for vehicle-mounted operations. Figure 16b depicts a possible 3x3 stacked geometry.

5.2 Multiple Source Simulation

In real-life application, there are scenarios where identification of multiple sources is necessary. The sources may not necessarily be the same source, nor would they have the same activity level. They could be arbitrarily placed, and ability to separate different sources is important for the imager. As mentioned in Section 2.1.2, using GPS within GEANT4 framework, multiple sources of arbitrary activity and location can be simulated.

Figure 17 demonstrates this capability, showing a simulated image of two ^{137}Cs sources placed 10 degrees from each other, with one source having half the activity of the

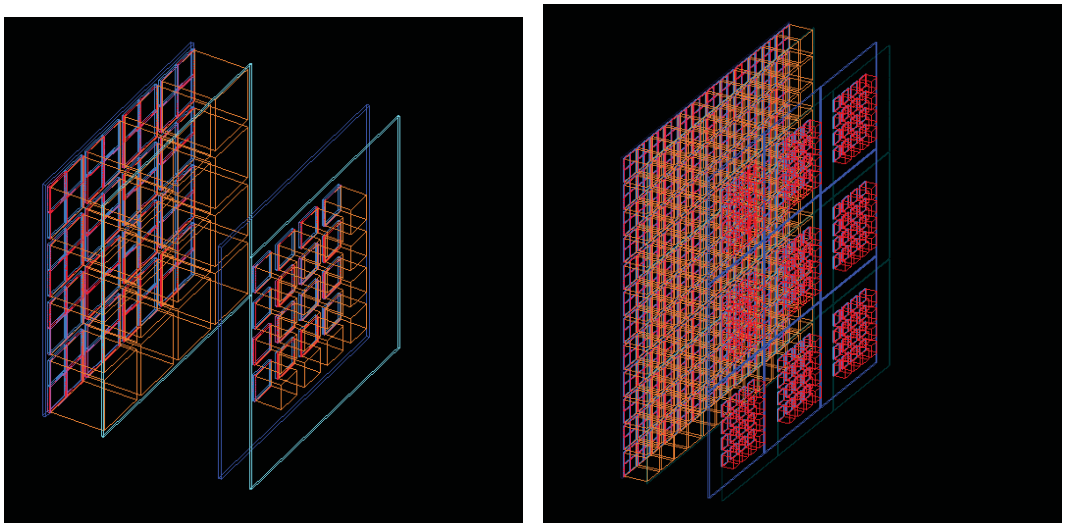

(a) ***(b)***

Figure 16: *A GEANT4 visualization of a mission-ready detector geometry. (a) depicts a single module; (b) depicts a 3 by 3 stacked configuration for increased sensitivity.*

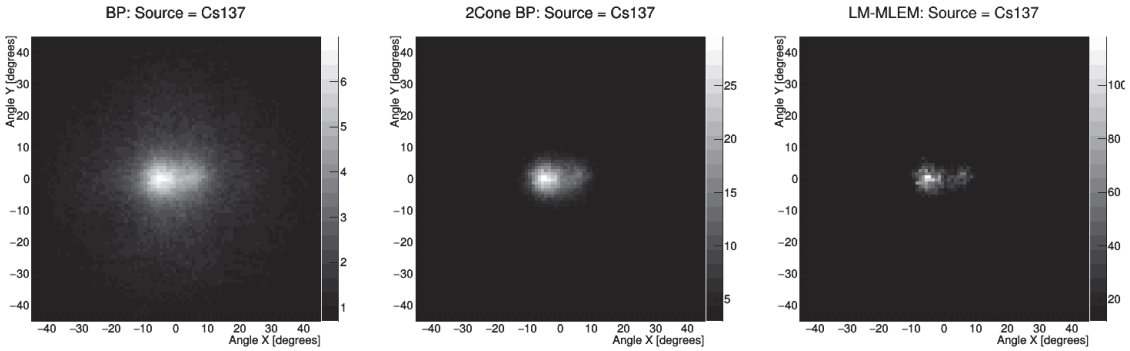

Figure 17: *Images of two sources located 10 m away from the detector and separated by 10 degrees from each other, obtained by simple back projection (left), two-cone back projection (centre) and LM-MLEM (right). The right source has half the activity of the left one*

other. As expected, the weaker source exhibits a dimmer signal. Ability to simulate multiple sources allows more robust evaluation of the image reconstruction algorithms introduced in Section 4. Figure 18 shows a test of imager's ability to resolve point sources separated by a known amount. None of the algorithms were able to resolve the two sources separated by 5 degrees (two right-most sources). It can be qualitatively concluded that LM-MLEM method best separates the sources, followed by the two-

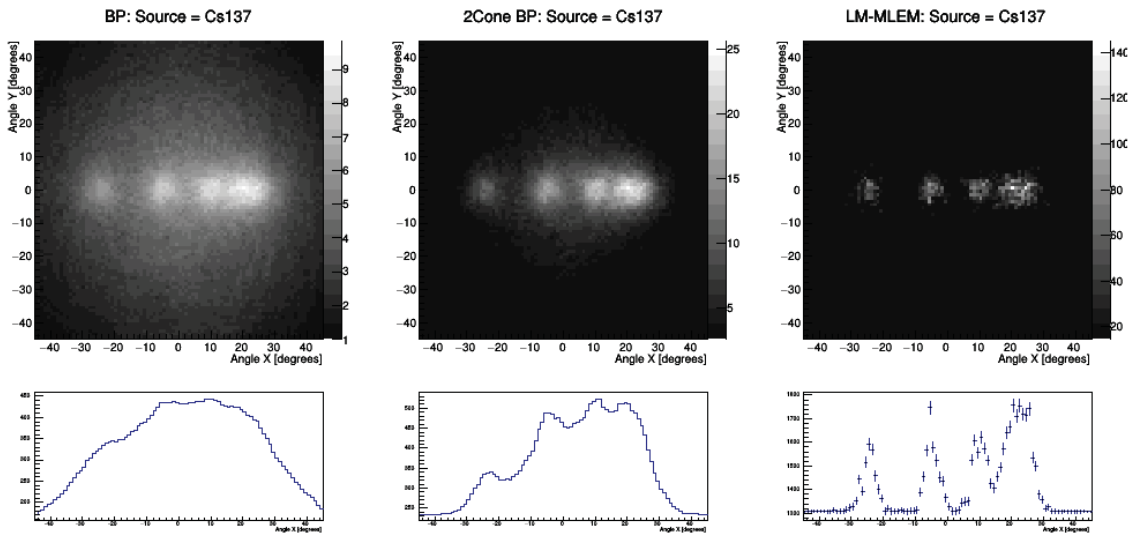

Figure 18: *Images of 5 point sources having the same activity, placed at (-25, -5, 10, 20, 25) degrees along the x-axis. The bottom plots show the intensity plot projected along the x-axis.*

cone back projection. The projection plot of the intensity as shown on the bottom of Figure 18 could be used to quantitatively evaluate the goodness of the separation. Quantitative analysis is still in progress.

5.3 Moving Source Simulation

In some cases, either the source or the detector is not static. An example of such scenario is a surveillance mission where vehicle-mounted detector moves through an area. In order to simulate such scenario, a modification is made in the simulation such that the source moves with respect to the detector.

An example of this is depicted in Figure 19, a series of back projection image of a 10 mCi point source moving from -30 degrees off-axis to +30 degree at a constant speed of 2 km/h (approximately 3 degrees/s). The source is located at 10 m from the detector at the point of closest approach. Even with the low statistics (approximately 30 events were collected within a 1-second window), the movement of the source is visible. This demonstrates the tracking capability of the detector of a moving source.

5.4 Extended Source Simulation

Extended source refers to a source that is not localized. A possible scenario including this type of source is a spill of contaminated liquid containing radioactive material,

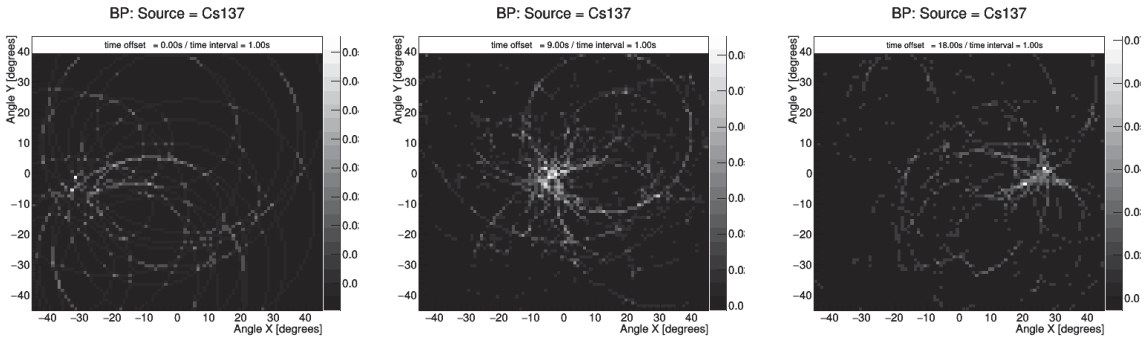

(a) ***(b)*** ***(c)***

Figure 19: *Simulation of a point source located 10 m away from the detector moving at 2 km/h and imaged within 1-second window using a simple back projection. (a) at $t = 0$ s the source is -30 degrees off-axis; (b) at $t = 9$ s the source is approximately in the middle; (c) at $t = 18$ s the source is -30 degrees off-axis.*

for example at a compromised nuclear reactor site. In this case, the imager is required to identify the extent of the spill, and the intensity of radioactivity. Extended source is also useful in evaluating the image reconstruction algorithms to see how well they can reconstruct the original shape.

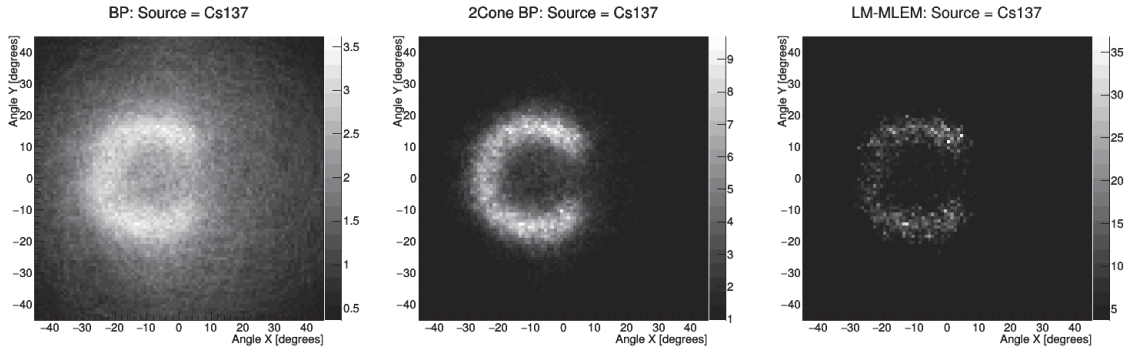

Figure 20: *Images of a C-shaped distribution using the three imaging algorithms. The centre of the C-shape is located at -10 degrees off-axis, and 10 m away from the detector. Te arc of the C-shape is 3 m in radius, and has opening of ∼40 degrees to the right.*

To demonstrate the capability of creating an extended source within GEANT4 simulation, a "C" shape is drawn and reconstructed using the Compton imager. Figure 20 shows the result of the three algorithms. All three algorithms are capable of reconstructing the original "C" shape. The two-cone algorithm produces sharper image compared to the simple back projection, and LM-MLEM algorithm further reduces

the noise around the shape, especially inside of the “C” arc.

6 Summary and Conclusions

Development of a Compton gamma imager is an on-going effort at DRDC with collaboration with NRC and NRCan. The work detailed within this report continues the previous effort, and further improved the GEANT4 simulation of the imager. The updated DRDC simulation package underwent a thorough scrutiny by comparing with the independently-developed NRC simulation package, where further improvement were made. Review of image reconstruction algorithms followed, namely simple back projection, two-cone backprojection, and LM-MLEM. Each of these algorithms were implemented and some preliminary evaluation were done. Lastly, several additional updates to the DRDC simulation packages were detailed, including addition of the mission-ready imager geometry, and added capability of multiple, moving, and extended sources.

There exist several items whose attention are needed:

- The discrepancy in the ARM distribution between GEANT4 version 4.9.6 and 4.10.1 is still unresolved. More study is needed to identify the source of this discrepancy
- Development of a quantitative analysis of the images produced by the reconstruction algorithms. So far the quantitative analysis has been done on a single point source scenarios
- Modelling of background signals. These originate from soil and other materials which are naturally occurring. A proper simulation using GEANT4 is necessary
- Modelling of detector response and propagation of uncertainties. Thus far a perfect detector response is assumed, and that the reconstructed Compton cones have no uncertainty. In reality the detector response is non-uniform (i.e. s_j in Equation 4), and Detector uncertainties affect the Compton angle (See Equation 1)

The above items will be addressed as the project goes forward, with additional cross checks from the project collaborators.

References

[1] Phillips, G., Gamma-ray imaging with Compton cameras, *Nuclear Instruments and Methods in Physics Research B*, 99(1995), 674–677.

[2] Saull, P. et al., First demonstration of a Compton gamma imager based on silicon photomultipliers, *Nuclear Instruments and Methods in Physics Research A*, 679(2012), 89–96.

[3] Sinclair, L. et al., Silicon Photomultiplier-Based Compton Telescope for Safety and Security (SCoTSS), *Proc IEEE Trans. Nucl. Sci.*, 61(2014), 2745 – 2752.

[4] Lam, J. (2015), SCoTSS Geant4 Design and Simulation, (DRDC-RDDC-2015-C113) Defence Research and Development Canada – Ottawa Research Centre.

[5] Agostinelli, S. et al., Geant4 - a simulation toolkit, *Nuclear Instruments and Methods in Physics Research Section A: Accelerators, Spectrometers, Detectors and Associated Equipment*, 506(2003), 250 – 303.

[6] Allison, J. et al., Geant4 developments and applications, *IEEE Transactions on Nuclear Science*, 53(2006), 270–278.

[7] Brun, R. and Rademakers, F., ROOT - An Object Oriented Data Analysis Framework, *Nucl. Inst. & Meth. in Phys. Res. A*, 389(1997), 81–86. See also http://root.cern.ch/.

[8] Geant4 General Particle Source (online), CERN, https://geant4.web.cern.ch/geant4/UserDocumentation/UsersGuides/ForApplicationDeveloper/html/ch02s07.html (Access Date: December 21, 2015).

[9] EGSnrc: software tool to model radiation transport (online), National Research Council Canada, http://www.nrc-cnrc.gc.ca/eng/solutions/advisory/egsnrc_index.html (Access Date: December 21, 2015).

[10] Knoll, G. (2000), Radiation Detection and Measurement, Wiley.

[11] Wilderman, S. et al., List-mode maximum likelihood reconstruction of Compton scatter camera images in nuclear medicine, *Proc IEEE Nuclear Science Symposium*, 3(1998), 1716 – 1720.

[12] Barrett, H. H., White, T., and Parra, L. C., List-mode likelihood, *J. Opt. Soc. Am. A*, 14(1997), 2914–2923.

[13] Parra, L. and Barrett, H., List-mode likelihood: EM algorithm and image quality estimation demonstrated on 2-D PET, *IEEE Transactions on Medical Imaging*, 17(1998), 228–235.